Date of publication xxxx 00, 0000, date of current version xxxx 00, 0000.

Digital Object Identifier 10.1109/ACCESS.2017.DOI

Analysis of Vertical Loop Antenna and Its Wide and Flat Variant Performance in Wearable Use

MARKUS BERG [1], (MEMBER, IEEE,), JIANGCHENG CHEN [1], (STUDENT MEMBER, IEEE,) AND AARNO PÄRSSINEN [1], (SENIOR MEMBER, IEEE)

[1]Centre for Wireless Communications, Faculty of Information Technology and Electrical Engineering, University of Oulu, Finland (e-mail: markus.berg@oulu.fi)

Corresponding author: Markus Berg (e-mail: markus.berg@oulu.fi).

"This work was done in WERME research project financially supported by Hilla research program through Tekes – the Finnish Funding Agency for Innovation."

ABSTRACT This paper presents an analysis of the input impedance and radiation pattern behavior for a rectangular loop antenna when it is reshaped from a narrow square to wide and flat. The antenna operation is examined by 3D electromagnetic simulations. Parametric simulation results are shown to explain the effect of antenna dimensions on the impedance behavior. Based on the numerical results, an equivalent circuit is developed to model the impedance change due to reshaping the loop antenna. The main observations are that the decreased height and the increased width of the antenna increase the bandwidth potential of the inherently narrowband loop and increase its directivity. These characteristics together with a vertical loop orientation enable a high performance antenna for locations very close to conductive or lossy materials. Based on the presented impedance analysis, an optimized antenna prototype for a wearable use is manufactured and its performance is verified by measurements. Measured radiation efficiency for the antenna in contact with a human tissue phantom is -5.0 dB at 2 GHz and the obtainable bandwidth potential is > 10 %.

INDEX TERMS equivalent circuit, loop impedance, small loop, user influence

I. INTRODUCTION

LOOP antenna is one of the basic radiator structures, with a comprehensive theoretical explanation found e.g. in [1]. Impedance of a circular thin-wire loop antenna has been theoretically examined by using Fourier series method which yielded numerical solutions for the impedance [2]. Now, the development of computational electromagnetic software has reduced the need of the complex theoretical approach for various and arbitrary loop shapes. In addition, numerical methods, e.g. FDTD (Finite Difference Time Domain), are efficient tools for evaluating antenna structures and can be used to increase the theoretical understanding of antenna behavior.

Electrically small loop antennas are often used for receiving broadcasted EM waves or as a magnetic field probes [3] at low frequencies because of their compact size. The low efficiency of the small loop is not disastrous in reception, since loop maintains the signal to noise ratio. In the modern wireless communication, loop based antenna solutions are used as a coupling element to the mobile device chassis or as a miniaturized and even frequency reconfigurable antennas [4]. Loop has been proposed also as internal FM receiving antenna for mobile devices [5].

Recently, wearable antennas have been extensively studied and they can be classified either for on-body or off-body antennas according to their purpose of use. On-body antennas are aimed for WBAN (Wireless Body Area Network) use e.g. in sensing applications, where the ability to wake up the surface wave propagation [6], the lateral gain [7] and the propagation around the human body [8] are critical. Wearable antennas for off-body communication are discussed in [9] covering a wide range of different antenna solutions showing the recent development of bendable and conformal antennas.

The performance of wearable antennas can be poor because of the lossy tissue. Earlier investigations show a high absorption to the tissue, e.g. in [10], but increased efficiency due to the shielding effect of the ground plane [11]. An efficient antenna typically has a ground plane to reduce

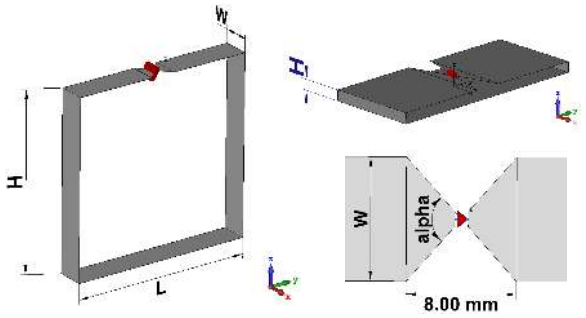

FIGURE 1. Square loop antenna (left), flat and wide loop (top right) and the feeding area tapering (bottom right).

radiation toward tissue [12]. This has a positive effect on the maximum gain but usually reduces the bandwidth potential of the antenna. Recently, a bracelet antenna having high electric field between two planar conductors has became public [13]. The operation of the antenna structure is discussed more detailed in [14].

The antenna structure analyzed in this paper is partly originated from [13] but the shape of an Inverted-F Antenna (IFA) is now developed to the form of a loop. Analysis of the impedance behavior begins with a square loop antenna and is described in Section II. Parametric studies for the loop antenna height and width are performed in Sections III and IV resulting impedance and radiation pattern changes. Equivalent circuit for the proposed loop is discussed in Section V and finally Section VI describe the bandwidth potential, the effect of a human tissue on the loop and the fabricated prototype together its measurement results.

II. SQUARE LOOP ANTENNA

Starting point of this study is a square loop antenna with the height of H and the length of L, depicted in Fig. 1. The loop circumference is $C = 2 \times (H + L)$ and for the numerical calculations a physical circumference of $C = 0.24$ m is used. Feed point of the antenna is in the middle of the one side, shown in Fig. 1. The feed area with the length of 8 mm is tapered toward the feed gap of 1 mm. The feed tapering angle is a function of the loop width W and follows $\alpha = 2 \times tan^{-1}(\frac{W/2}{4})$. Loop conductor is formed of an extremely thin strip with a perfect conductivity. The square loop antenna was modelled and its operation was simulated using the time domain solver in CST Studio Suite. Analysis of the antenna operation was examined mainly through the antenna input impedance Z. The loop is a multi-resonant antenna by nature and the analysis was conducted for loop circumference from $C = 0\lambda$ to 3.2λ. Corresponding frequency range is from 0 to 4 GHz for the given physical circumference.

A. EFFECT OF THE LOOP WIDTH ON INPUT IMPEDANCE Z

The input resistance R and reactance X are depicted in Fig. 2 and Fig. 3 as a function of circumference in wavelengths for different W values. The resonances of the loop follow

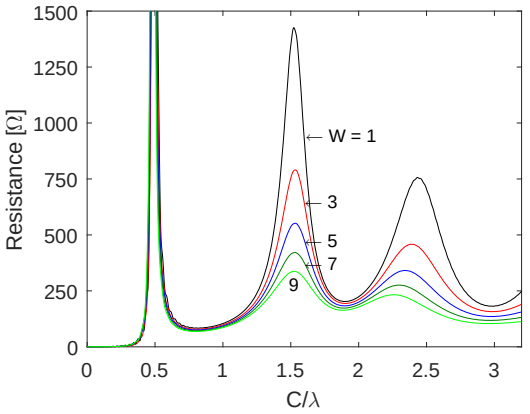

FIGURE 2. Effect of the square loop width w on the loop resistance.

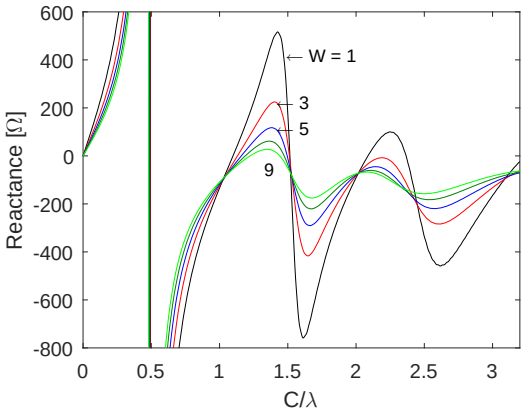

FIGURE 3. Effect of the square loop width w on the loop reactance.

integer values of C/λ and anti-resonances occur half way between these integer values, described in detail in [15]. The very high and rapid variation of the resistance and reactance is characteristic for the anti-resonance [1]. The behaviour follow the corresponding ones of a circular thin-wire loop antenna [2], although originated from a different loop shape. It is observed, that resistance and reactance of the first anti-resonance are relatively stable for any W value, whereas in case of second and third anti-resonances they are subject to large variations. Increasing W from 1 mm to 9 mm decreases the resistance of the second anti-resonance from 1400 Ω to 300 Ω and diminishes reactance variation. For the third anti-resonance when $C = 2.5\lambda$ the behaviour is similar except the decrease of R from 750 Ω to 230 Ω and the shift of the maximum resistance value for 0.18 λ lower frequency. Thus, the quality factors of the second and third resonances are decreased.

B. RADIATION PATTERNS AND E-FIELD DISTRIBUTION

The radiation pattern of the loop antenna changes from omnidirectional to directional depending on the circumference of the loop. Illustrated elevation plane radiation patterns for

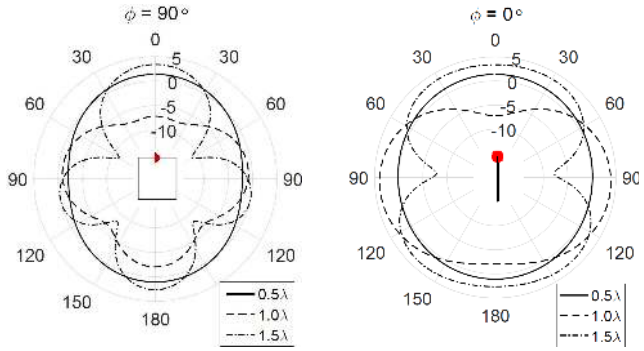

FIGURE 4. Elevation plane directivity patterns [dBi] of the vertically oriented square loop for $\phi = 90°$, and $\phi = 0°$ ($C = 0.5\lambda, 1.0\lambda$ and 1.5λ).

narrow loop ($W = 1$) are shown in Fig. 4 for $C = 0.5\lambda$, $C = 1.0\lambda$ and $C = 1.5\lambda$ for azimuthal angle $\phi = 90°$, i.e. in the plane of the loop, and for $\phi = 0°$. Radiation pattern of the half-wavelength loop is omnidirectional. Due to the increased electrical circumference of the loop, multiple beams and increased directivity are observed. The electric field maximum occurs over the feed gap for two first anti-resonance modes. Field minimum is found opposite to the feed of the loop. This minimum is frequency independent and is due to the uneven number of E-field maxima of the symmetrically excited square loop antenna.

III. FLATTENING THE NARROW LOOP (TOWARD FOLDED DIPOLE)

The circumference of the square loop antenna in the first anti-resonance is $C = 0.5\lambda$. Simulations with dimensions $H = 60$ mm, $L = 60$ mm and $W = 1$ mm yield to the resonance frequency of 616 MHz where free-space wavelength equals 243 mm, being very close to the circumference C. Flattening of the loop antenna is implemented by decreasing the loop height H from 60 mm to 10 mm, while keeping L and W constant. The antenna structure is actually a folded dipole antenna when the loop width is small [16]. The frequency domain resonance behaviour is depicted by means of the loop resistance and shown in Fig. 5. It is obvious that resonances move toward higher frequencies as the electrical length of the loop decreases. The peak R value of the first anti-resonance decreases rapidly as H goes smaller. The peak value of the second resonance varies between $R = 800...1400\ \Omega$, as shown in Fig. 5. Corresponding change of X is small, but for the second and third anti-resonances (for square loop shown in Fig. 3), a slightly reduced phase change of the input impedance is observed due to flattening the loop (H decreases). This is deduced from the smaller reactance extremum values and can be seen more easily on Smith chart.

Resistance and reactance for flattened loop with heights $W = 3$ mm and 10 mm are shown in Fig. 6. Reducing the height below 10 mm influence an increase in R of the second anti-resonance (close to 3 GHz). In the resonance (around 2 GHz) it equals 250 Ω being relatively constant over frequency band of 500 Mhz. The slope of X is stable for the

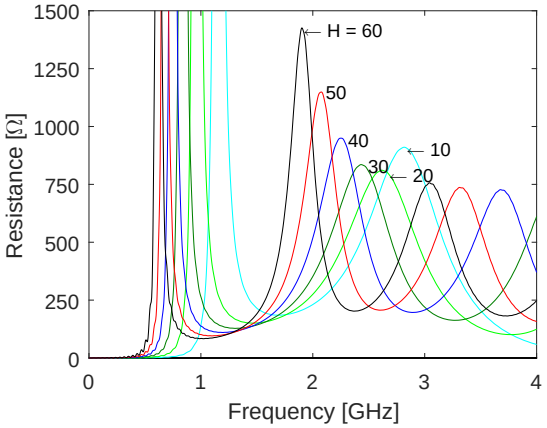

FIGURE 5. Effect of the loop height H (10…60 mm) on the loop resistance, when $W = 1$ mm and $L = 60$ mm.

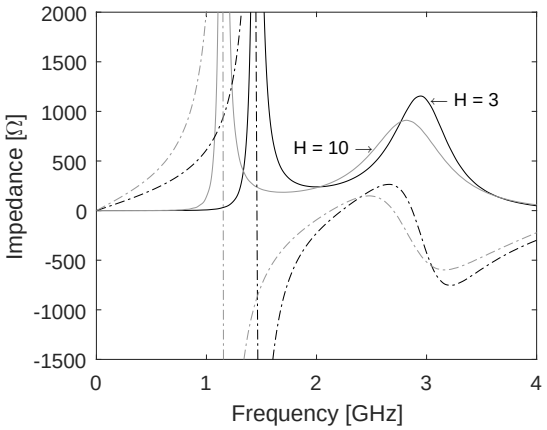

FIGURE 6. Real (—) and imaginary (– · –) impedance of two resonances of the flat loop ($L = 60$ mm, $W = 1$ mm).

same range. With a proper matching circuit this impedance behaviour enables rather wideband matching and is thus attractive for practical applications.

At 2 GHz, as the height H of the loop is decreased, the radiation pattern transforms toward omnidirectional. This is due to the loop circumference shortening below λ and the square shape deformation toward a folded dipole. Because of the parallel electric currents in the folded dipole, it operates in the antenna mode [17].

IV. WIDENING THE FLAT LOOP ANTENNA

Because of the promising impedance, the loop antenna height $H = 3$ mm was selected for investigation of the influence of the loop width W variation on the input impedance and radiation properties. Simulated resistance changes for $W = 5 - 50$ mm are shown in Fig. 7. The resistance of the narrowest loop at $\lambda/2$ is $R \approx 300\Omega$ and follows that of the folded dipole [16]. It is observed that the peak values of the first and second anti-resonances start to diminish gradually when increasing the loop width, and finally merge with each

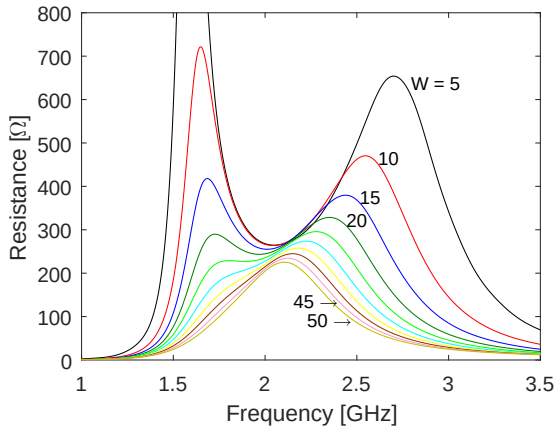

FIGURE 7. Effect of the flat loop width W on the loop resistance, when $H = 3$ mm and $L = 60$ mm.

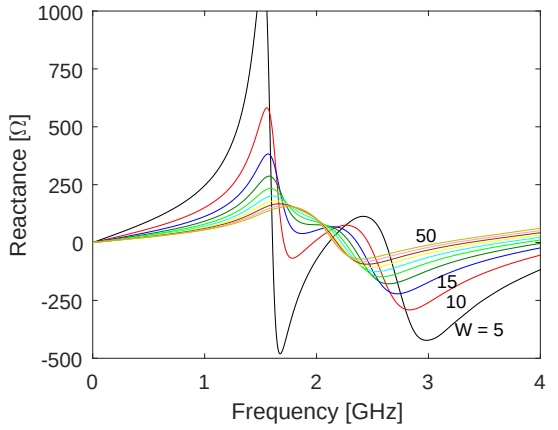

FIGURE 8. Effect of the flat loop width W on the loop reactance, when $H = 3$ mm and $L = 60$ mm.

other resulting one resonance with the peak R value of 225 Ω at 2.1 GHz. Increasing width actually reveals the original lowest $\lambda/2$-resonance, determined by the loop circumference. For comparison, the reactance changes are shown in Fig. 8, where the merging of these two resonances are seen as a gradual disappearance of the zero-reactance crossings of two anti-resonances. Observed slower frequency-domain phase change yield to the favourable input impedance.

Due to the increased width of the loop, the traditional current formulation of the loop, used e.g. in [15], is not valid anymore. Instead of one current approximation, two distinct surface current modes were found, which exist on the inner and the outer surfaces of the planar loop. The inner current is much stronger than the outer, and creates high E-field between planar conductor sections of the loop. Field distribution for different times are illustrated in Fig. 9. The E-field is strong over the feed gap and resembles that of a slot type of an antenna. It is observed that E-field minimum remains on the opposite side of the loop feed at any moment. This leads to insensitivity for closely located objects.

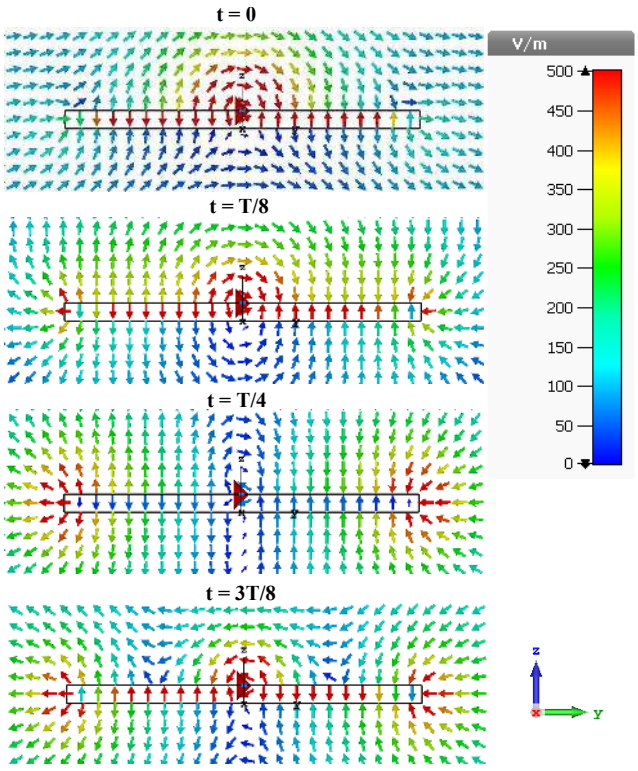

FIGURE 9. Simulated E-field distribution of the flat loop at 2 GHz for different times.

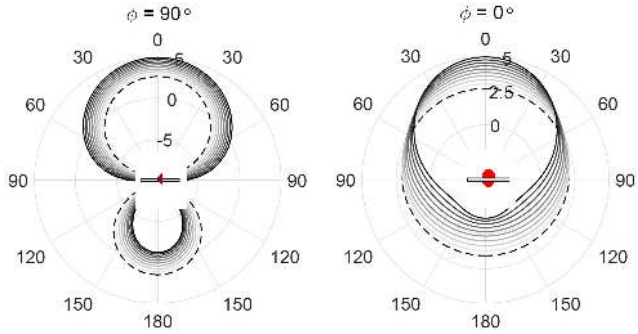

FIGURE 10. Effect of the flat loop width W on the elevation plane directivity patterns [dBi] for $\phi = 90°$ and $\phi = 0°$. $L = 60$ mm, $H = 3$ mm).

Due to the observed field minima, the radiation pattern becomes more directive. The elevation plane radiation patterns for $\phi = 90°$ and $\phi = 0°$ are shown in Fig. 10 for different loop widths $W = 5...50$ mm at 2 GHz. Maximum directivity of 5 dBi in the direction of the loop feed is achieved with the largest width. Simultaneously, directivity in the opposite direction decrease from 1.5 dBi to -1.2 dBi. This reasonably high directivity is beneficial for the antenna in the close proximity of lossy objects, such as human tissue.

V. EQUIVALENT CIRCUIT FOR SQUARE AND FLAT LOOPS

In order to understand the loop behaviour, an equivalent circuit for the loop was derived. First resonance is modelled

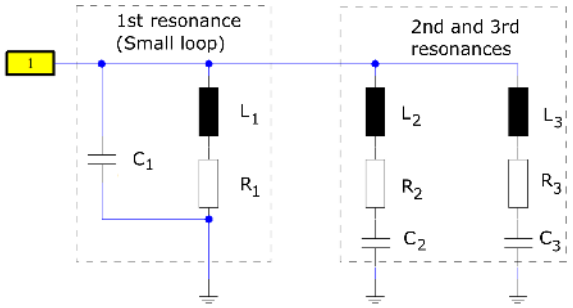

FIGURE 11. Equivalent circuit for the loop.

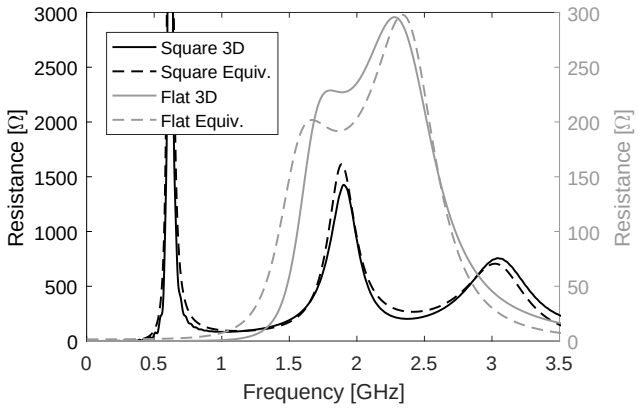

FIGURE 12. Simulated resistance graphs for square and flat loops using 3D and circuit models.

as series LC-circuit commonly used for small loops [1] and shown in Fig. 11. Resistance and inductance of the loop are generated by R_1 and L_1 whereas a shunt capacitance C_1 is used to eliminate the reactive impedance caused by L_1. Higher order resonances are modelled using two series RLC-circuits which are parallel to the small loop equivalent. Each R include radiation and loss resistances of the particular resonance.

Resistance curves of the square loop obtained by 3D EM- and equivalent circuit simulations are shown in Fig. 12. The dimensions for the square loop are $H = L = 60$ mm, and $W = 1$mm. The applicability of the equivalent circuit is confirmed by comparing the corresponding resistance curves of the flat and wide loop antenna, also shown in Fig. 12. Dimensions for the flat loop are $H = 3$ mm, $L = 60$ mm, and $W = 25$ mm. The equivalent circuit component values for both antennas are listed in Table 1. The high L_1, L_2 and L_3 values are due to the inductive nature of the loop antenna.

It is observed that the three-resonance equivalent circuit response follow the 3D-simulation results with reasonable accuracy. The role of the resistor values is important in order to achieve a proper resistance level between resonances. The resistor value of the individual resonator determines the adjacent lower frequency resistance level together with the related capacitor value. The equivalent circuit inductor values

TABLE 1. Equivalent circuit component values, $R[\Omega]$, $C[\mathrm{pF}]$, $L[\mathrm{nH}]$

Component	Square loop	Flat loop
R_1	0.78	1.55
C_1	0.15	0.8
L_1	172	8.0
R_2	113	208
C_2	0.17	0.22
L_2	87	31.7
R_3	460	-
C_3	0.03	-
L_3	118	-

determine locations of individual resonances together with the series capacitors. The maximum resistance values are determined by relative inductor values.

In case of the flat and wide loop antenna, only two lowest resonance circuits of the equivalent are used. Based on the simulated impedance, it is clear that the decreased height together with the increased width of the sheet influence a rapid decrease in inductance values. For the first resonance this means reduction from 172 nH to 8 nH. Although larger capacitance between the inner surfaces of the loop, only small increase in capacitance values is found, as shown in Fig. 12 and Table 1. Resistance values R_1 and R_2 are doubled in comparison with those of the square loop.

VI. FLAT LOOP CLOSE TO HUMAN TISSUE

The performance of the flat and wide loop antenna in close proximity of the human tissue was investigated by 3D simulations. Three flat loops ($H = 3$ mm) of different widths $W = 1, 5$, and 25 mm close to a tissue block were modelled using CST Studio Suite. The size of the tissue block was 80 mm x 140 mm x 30 mm. Electrical material parameters of the tissue followed CTIA standard for mobile device measurements, with ϵ_r being 27 - 24.8 and $tan\ \delta$ being 0.37 - 0.39 over the band of interest (1.7 - 2.2 GHz) [18]. A sheet of cardboard was used as the loop substrate, filling the gap between loop wires. The prototype simulations were performed using copper for conductive part and cardboard as a substrate ($\epsilon_r = 1.78, tan\ \delta = 0.02$) [19]. The length of the loop ($L = 60$ mm) was constant for all antennas.

A. TISSUE INFLUENCE ON IMPEDANCE AND EFFICIENCY

Antennas were modelled on top of the tissue block, with a distance $d = 0 - 12$ mm between the surface of the tissue and the bottom of the loop. Simulation setup is depicted in Fig. 13 for the widest loop.

Simulated resistances for the widest loop ($W = 25$ mm) with different distances d are shown in Fig. 14. A clear resonance frequency shift from 1.56 GHz to 1.74 GHz is observed due to the capacitive loading of the tissue. Frequency detuning is now toward higher frequency, unlike the typical down-tuning in case of the electrical wire antennas. The detuning can be seen in Fig. 15 depicting impedance loci on Smith chart. Impedance on contact with tissue is shown

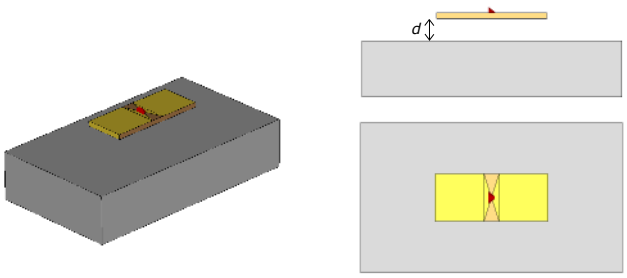

FIGURE 13. Oblique (left), side and top views (right) of the simulation model for flat loop close to a tissue block.

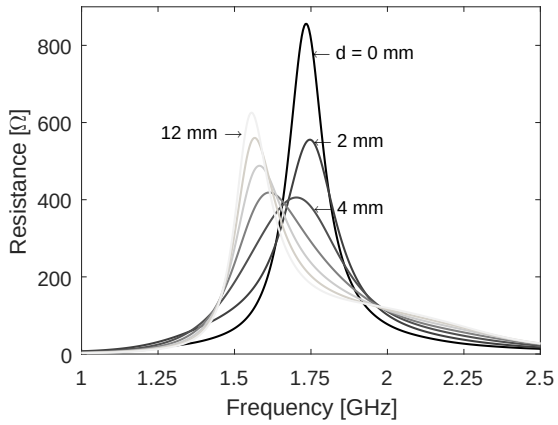

FIGURE 14. Flat loop resistance as a function of distance d to tissue.

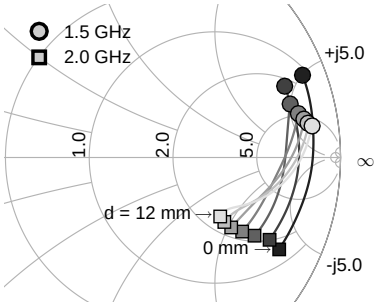

FIGURE 15. Flat loop impedance loci on Smith chart describing frequency detuning due to decreased d.

as black line over the frequency range of 1.5 - 2.0 GHz and gradual 2 mm increase of the distance d is illustrated by fading grey shades. At 1.5 GHz the decreased distance decreases both the input inductance and the input resistance which then cause constant frequency point movement away from resistance axis. This is shown as a movement of the circular marker in Fig. 15. Above the resonance, i.e. on the capacitive side of the chart, impedance variation follows approximately the constant resistance curve.

The radiation efficiency of the antenna η_{rad} describes the maximum achievable total efficiency in case of perfect lossless matching. It is a good figure of merit for on-body

FIGURE 16. Antenna prototype with coaxial feeding bent around the loop (left) and the on-body measurement setup (right).

antennas describing the losses caused by absorption to the tissue. The simulated η_{rad} for different distances d are shown in Table 2 for three different loop widths (W = 1, 5 and 25 mm). Widening the loop results in a radiation efficiency increase from -10.9 dB to -4.9 dB when antenna is touching tissue. The shielding effect of the wide loop is clearest for small distances and decrease as the distance increases.

TABLE 2. Simulated and measured radiation efficiencies [dB] as a function of loop width and distance to tissue at 2 GHz

	d[mm]							
W[mm]	0	2	4	6	8	10	12	fs
1	-10.9	-9.7	-8.6	-7.4	-6.3	-5.2	-4.3	-0.1
5	-8.5	-8.3	-7.6	-6.8	-5.8	-4.9	-4.1	-0.1
25	-4.9	-4.7	-4.7	-4.4	-3.9	-3.4	-2.9	-0.3
24 (meas.)	-5.0	-	-	-	-	-	-	-1.0

In order to compare the measured radiation efficiency to the simulated one, which is easily extracted from 3D EM-simulator, the radiation efficiency η_{rad} can be calculated from the measured S_{11}-parameters and the measured total efficiency η_{tot} using equation

$$\eta_{rad} = \frac{\eta_{tot}}{1 - |S_{11}|^2}. \quad (1)$$

B. PROTOTYPE

In order to verify the simulated performance, a flat loop antenna prototype with dimensions of $H = 3$ mm, $L = 60$ mm, and $W = 24$ mm was manufactured and is shown in Fig. 16. Conductive material is a standard copper tape and the coaxial feeding cable was bent and soldered around the perimeter of the loop in order to minimize the cable effect. Location of the coaxial cable detaching point was selected due to the electric field minima opposite to the antenna feed. Regardless of the symmetrical antenna structure, balun was not implemented to balance the antenna currents. Cardboard was used as substrate material and its inhomogeneous internal structure was modelled using relative permittivity of paper ($\epsilon_r = 3.85$) and air ($\epsilon_r = 1$).

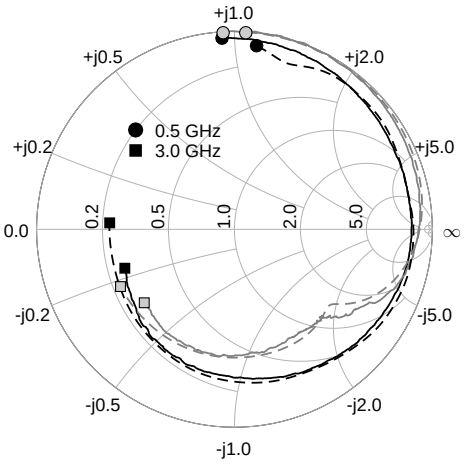

FIGURE 17. Measured (—) and simulated (- - -) S_{11}-parameters of loop antenna. Grey colour is for free space and black for on-body located antenna.

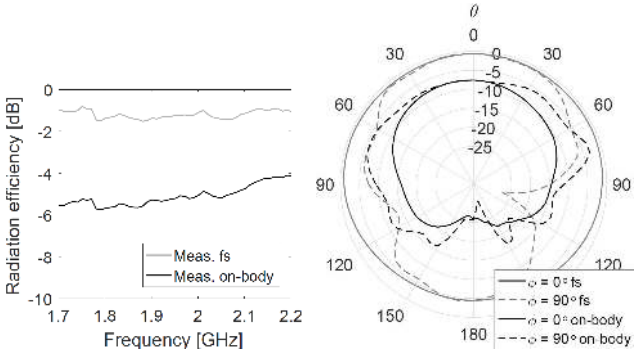

FIGURE 18. Measured radiation efficiency (left) and measured elevation plane gain patterns [dBi] for free space and on-body cases (right).

C. MEASUREMENT RESULTS

Prototype was measured in free space and with a hand phantom, shown in Fig. 16. Measured S_{11}-parameters for the loop are shown on Smith chart in Fig. 17 together with the simulated ones. During measurement a port extension of 110 mm was used in order to remove the phase change due to the coaxial feed cable. Measured and simulated impedance loci are very close to each other, and correspond the loading effect of the human hand phantom shown in Fig. 15. The radiation efficiencies based on measurements and Eq. (1) are shown in Fig. 18 and a comparison with simulated results is shown in Table 2. At 2 GHz the measured radiation efficiencies with and without phantom were -5.0 dB and -1.0 dB, respectively, being very close to the simulated values.

The measured elevation plane radiation patterns are shown in Fig. 18 for azimuth angles $\phi = 0°$ and $\phi = 90°$. The prototype did not include matching circuits which yield to low gain. However, the shape of the free space radiation pattern is very close to the simulated (Fig. 10) and the overall performance can be evaluated based on the measured radiation efficiency.

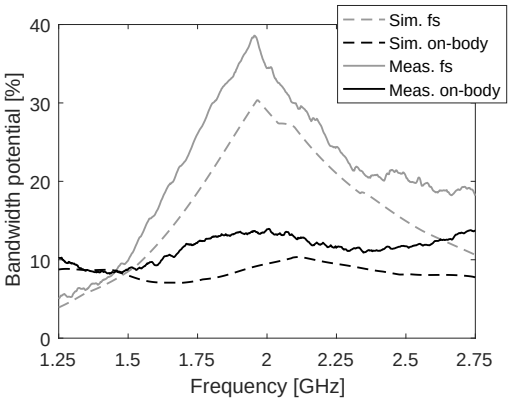

FIGURE 19. Bandwidth potential for the simulated and measured flat loops with the cardboard substrate.

The obtainable impedance bandwidth of the loop was evaluated through a concept of bandwidth potential. A mathematically constructed lossless 2-component matching circuit was used to calculate the obtainable bandwidth using the method originally presented in [20] and explained in detail in [21]. Bandwidth potentials of simulated and measured flat loops were calculated by Optenni Lab software and are shown in Fig. 19 for free-space and for on-body ($d = 0$ mm) cases. Measured and simulated bandwidth potentials follow same trend but measured is always 0 - 8 percentage units higher. Difference is due to the manufacturing inaccuracy and material parameter deviation of the phantom prototype. In free-space, the bandwidth potential is high close to the targeted 2 GHz center frequency. For on-body case the decreased bandwidth potential is due to the loading effect of the human hand phantom. However, the flat loop can achieve over 10 % bandwidth potential over a wide frequency range even in contact with the human hand phantom. Combined with the thin antenna profile, the directional characteristics of the radiation pattern and the high radiation efficiency, these results enable high performance antenna structures for on-body applications.

VII. CONCLUSION

The rectangular loop antenna impedance and radiation pattern analyses have been conducted by 3D EM-simulations. The main emphasis has been on the loop impedance behaviour due to antennas shape transformation from a narrow square loop to a flat and wide. This transformation decreases the inductance and slowly increase the capacitance of two first resonances. Consequently, these resonances finally merge together and form advantageous resistance and reactance behaviour for the broadband impedance matching. In other words, the shape transformation increase the bandwidth potential of the loop. These observations are the main contributions of this work. In addition, two surface current distributions, inner and outer, were found and identified for the flat and wide loop.

For more detailed analysis, an equivalent circuit for three first resonances of the square-shaped loop antenna was derived. First resonance was modelled by a well-known small loop equivalent and two higher order resonances were modelled by parallel RLC circuits with a clear correspondence to the physical behaviour. Equivalent circuit component values for different widths and heights of the loop antenna were found.

The flat and wide loop antenna was found advantageous for the on-body usage because of its directional radiation pattern, shielding effect of the broadened loop sheet, and high bandwidth potential. Moreover, the wide loop form factor is beneficial for thin wearable devices and the antenna can achieve a high radiation efficiency even in contact with lossy hand tissue phantom.

ACKNOWLEDGMENT

The authors would like to thank WERME project partnering companies for the enthusiastic and fruitful collaboration, and especially Verkotan Oy for the radiation pattern and efficiency measurements.

REFERENCES

[1] C. A. Balanis, Antenna Theory, Analysis and Design, 3rd ed. John Wiley & Sons, Inc., 2005.
[2] J. E. Storer, "Impedance of thin-wire loop antennas," Transactions of the American Institute of Electrical Engineers, Part I: Communication and Electronics, vol. 75, no. 5, pp. 606–619, Nov 1956.
[3] M. Kanda, "Standard probes for electromagnetic field measurements," IEEE Transactions on Antennas and Propagation, vol. 41, no. 10, pp. 1349–1364, Oct 1993.
[4] H. Wang, Y. Wang, J. Wu, P. Chen, Z. Wu, C. Y. D. Sim, and G. Yang, "Small-size reconfigurable loop antenna for mobile phone applications," IEEE Access, vol. 4, pp. 5179–5186, 2016.
[5] P. Lindberg and A. Kaikkonen, "Internal active antenna for FM radio reception in mobile handsets," in The Second European Conference on Antennas and Propagation, EuCAP 2007, Nov 2007, pp. 1–10.
[6] M. Grimm and D. Manteuffel, "Norton surface waves in the scope of body area networks," IEEE Transactions on Antennas and Propagation, vol. 62, no. 5, pp. 2616–2623, May 2014.
[7] M. Berg, T. Tuovinen, and E. T. Salonen, "Low-profile antenna with optimal polarization for 2.45 GHz on-body sensor nodes," in 2014 Loughborough Antennas and Propagation Conference (LAPC), Nov 2014, pp. 641–643.
[8] G. A. Conway and W. G. Scanlon, "Antennas for over-body-surface communication at 2.45 GHz," IEEE Transactions on Antennas and Propagation, vol. 57, no. 4, pp. 844–855, April 2009.
[9] P. Nepa and H. Rogier, "Wearable antennas for off-body radio links at VHF and UHF bands: Challenges, the state of the art, and future trends below 1 GHz." IEEE Antennas and Propagation Magazine, vol. 57, no. 5, pp. 30–52, Oct 2015.
[10] S. Amendola, S. Milici, and G. Marrocco, "Performance of epidermal RFID dual-loop tag and on-skin retuning," IEEE Transactions on Antennas and Propagation, vol. 63, no. 8, pp. 3672–3680, Aug 2015.
[11] S. W. Su and Y. T. Hsieh, "Integrated metal-frame antenna for smartwatch wearable device," IEEE Transactions on Antennas and Propagation, vol. 63, no. 7, pp. 3301–3305, July 2015.
[12] T. Tuovinen, M. Berg, W. G. Whittow, and E. T. Salonen, "Performance of WBAN on-ground antenna type with relation to analytical path loss model," in 2014 Loughborough Antennas and Propagation Conference (LAPC), Nov 2014, pp. 55–59.
[13] P. Miskovský, "Antenna device and wearable device comprising such antenna device," Patent US 2 016 006 111, July, 2016.
[14] M. del Rosario Llenas, "Study of antenna concept for wearable devices," M.Sc.Thesis, KTH Royal Institute of Technology, 2015.
[15] A. F. McKinley, T. P. White, I. S. Maksymov, and K. R. Catchpole, "The analytical basis for the resonances and anti-resonances of loop antennas and meta-material ring resonators," Journal of Applied Physics, vol. 112, no. 9, p. 094911, 2012.
[16] G. Thiele, E. Ekelman, and L. Henderson, "On the accuracy of the transmission line model of the folded dipole," IEEE Transactions on Antennas and Propagation, vol. 28, no. 5, pp. 700–703, Sep 1980.
[17] W. L. Stutzman and G. A. Thiele, Antenna Theory and Design, 3rd ed. John Wiley & Sons, Inc., 2013.
[18] CTIA, "Test plan for wireless device over-the-air performance, method of measurement for radiated RF power and receiver performance," 2015.
[19] H. Saghlatoon, L. Sydänheimo, L. Ukkonen, and M. Tentzeris, "Optimization of inkjet printing of patch antennas on low-cost fibrous substrates," IEEE Antennas and Wireless Propagation Letters, vol. 13, pp. 915–918, 2014.
[20] J. Villanen, J. Ollikainen, O. Kivekäs, and P. Vainikainen, "Coupling element based mobile terminal antenna structures," IEEE Transactions on Antennas and Propagation, vol. 54, no. 7, pp. 2142–2153, July 2006.
[21] J. Rahola, "Bandwidth potential and electromagnetic isolation: Tools for analysing the impedance behaviour of antenna systems," in 2009 3rd European Conference on Antennas and Propagation, March 2009, pp. 944–948.

MARKUS BERG (S'07–M'12) received the M.Sc. (Tech.) and D.Sc. degrees in electrical engineering from the University of Oulu,Oulu, in 2005 and 2011, respectively.

From 2005 to 2015 he was a Research Scientist and Project Manager with the Centre for Wireless Communications, University of Oulu. In 2015, he was a Design Engineer with Elektrobit, Oulu Finland, and Bittium, Oulu Finland. He is currently an Adjunct Professor with the Faculty of Information Technology and Electrical Engineering, University of Oulu. His current research interests include antennas and propagation for wireless communication, wearable and frequency tunable antennas for small devices, and GNSS radio channel characterization.

Dr. Berg has authored and co-authored more than 60 international journal and conference papers.

JIANGCHENG CHEN received the M.Sc. degree in Communication Engineering from the University of Manchester, UK, in 2013.

He is now working as a researcher and pursuing the doctoral degree in Centre for Wireless Communications, University of Oulu, Finland. His current research interests include wearable antenna, 5G mobile terminal antenna and metamaterials.

AARNO PÄRSSINEN (S'95–M'01–SM'11) received the M.Sc., Licentiate in Technology and Doctor of Science degrees in electrical engineering from the Helsinki University of Technology, Finland, in 1995, 1997, and 2000, respectively.

From 1994 to 2000 he was with Electronic Circuit Design Laboratory, Helsinki University of Technology, Finland, working on direct conversion receivers and subsampling mixers for wireless communications. In 1996, he was a Research Visitor at the University of California at Santa Barbara. From 2000 to 2011 he was with Nokia Research Center, Helsinki, Finland. During 2009-2011 he served as a member of Nokia CEO Technology Council. From 2011 to 2013, he was at Renesas Mobile Corporation, Helsinki, Finland working as a Distinguished Researcher and RF Research Manager. From October 2013 to September 2014 he was an Associate Technical Director at Broadcom, Helsinki, Finland. Since September 2014 he has been with University of Oulu, Centre for Wireless Communications, Oulu, Finland where he is currently a Professor. His research interests include wireless systems and transceiver architectures for wireless communications with special emphasis on the RF and analog integrated circuit and system design.

Prof. Pärssinen has authored and co-authored one book, one chapter of a book, more than 50 international journal and conference papers and holds several patents. He served as a member of the technical program committee of Int. Solid-State Circuits Conference in 2007-2017, where he was the chair of European regional committee in 2012-13, and the chair of the wireless sub-committee in 2014-2017. Since July 2015 he is serving as Solid-State Circuits Society representative for IEEE 5G initiative.